Volume 12, Number 2, 2019. pp. 113-132

Jordan Journal of Physics

ARTICLE

Basic Concepts and Development of Dry Deposition Modelling

Tareq Hussein, Safa' Ibrahim and **Sawsan Malek**

Department of Physics, The University of Jordan, Amman 11942, Jordan.

Received on: 31/1/2018; *Accepted on: 3/10/2018*

Abstract: Dry deposition is the primary mechanism by which suspended particles are transported from gas onto surfaces. Prediction of this transport rate represented by the dry deposition velocity (V_d) is needed in a vast range of applications, such as atmospheric climate and air quality models, industrial processes, nanomaterials, clean rooms, building engineering, particle losses inside sampling lines, health effect of atmospheric particles and pharmaceutics. The particle transport rate towards the surface depends on many factors: above-surface air flow and fluid characteristics, physical characteristics of the particles and surface properties. Although dry deposition models have been improved significantly, they still need to be further developed to improve the model accuracy and include weak mechanisms of particle transport. In general, a dry deposition model incorporates Fickian diffusion (Brownian and Eddy) and gravitational settling. Turbophoresis was introduced to compensate for the enhancement in V_d as a result of inhomogeneous turbulent mixing. In real-life conditions, electrophoresis and thermophoresis are not strong enough mechanisms to be included in model calculations, but for some applications (such as air purifiers), these transport mechanisms are very important to be considered in model formulation. Magnetophoresis, which is a very weak mechanism in real-life conditions, can be enhanced for certain industrial applications. In general, deposition surfaces are rarely smooth and researchers have put great efforts to describe surface roughness in dry deposition models. After all, a unified dry deposition formulation is needed to be developed/ improved in the future to make dry deposition prediction and calculations easier and more accurate. In this paper, we present the basic concepts that have been developed and implemented in dry deposition models and illustrate the effect of different processes on the transport rate of suspended particles in the fluids towards surfaces. As a benchmark for the accuracy of the current dry deposition modelling, we present a comparison between model calculations and experimental data-bases found in the literature.

Keywords: Fickian diffusion, Gravitational settling, Turbophoresis, Electrophoresis, Thermophoresis, Magnetophoresis.

1. Introduction

Particle deposition onto surfaces is an important phenomenon from many aspects. It has a wide of range applications, such as environmental, industrial, medical, … etc. The effectiveness of the deposition mechanism is usually represented by the dry deposition velocity (V_d), which is derived from the particle flux towards the surface across the so-called concentration boundary layer [1–4]. Above any type of surface, V_d depends on the physical properties of the deposited particle (such as particle size, shape, density, … etc.), fluid and air flow characteristics inside the concentration boundary layer and surface properties [5–14]. Detailed calculation of these features is not possible in practical applications, which calls for simple mathematical formulae for V_d [2].

The main challenge in calculating V_d, especially deriving a simple and accurate formula, is to find appropriate values for the

Corresponding Author: Tareq Hussein **Email**: t.hussein@ju.edu.jo

boundary-layer parameters (y_0 and y_{cbl}), which are depicted in Fig. 1. For a smooth surface, there is a well-known dependence of V_d on the particle size [2, 3, 14–20]. Above a rough surface, y_0 and y_{cbl} are shifted away from the surface, so that V_d is different from that above a smooth surface (Fig. 2). Accounting for surface roughness in model calculations is complicated, but it is extremely important.

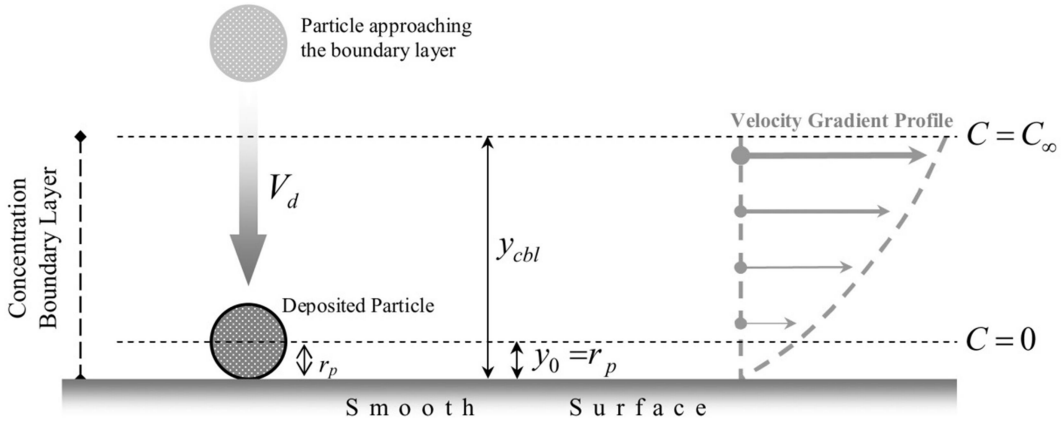

FIG. 1. Schematic illustration for the dry deposition of a particle (radius r_p) onto a smooth surface. The particle number concentration within the boundary layer is zero ($C = 0$) at y_0 and $C = C_\infty$ at y_{cbl}. *Figure was adopted from Hussein et al. [12].*

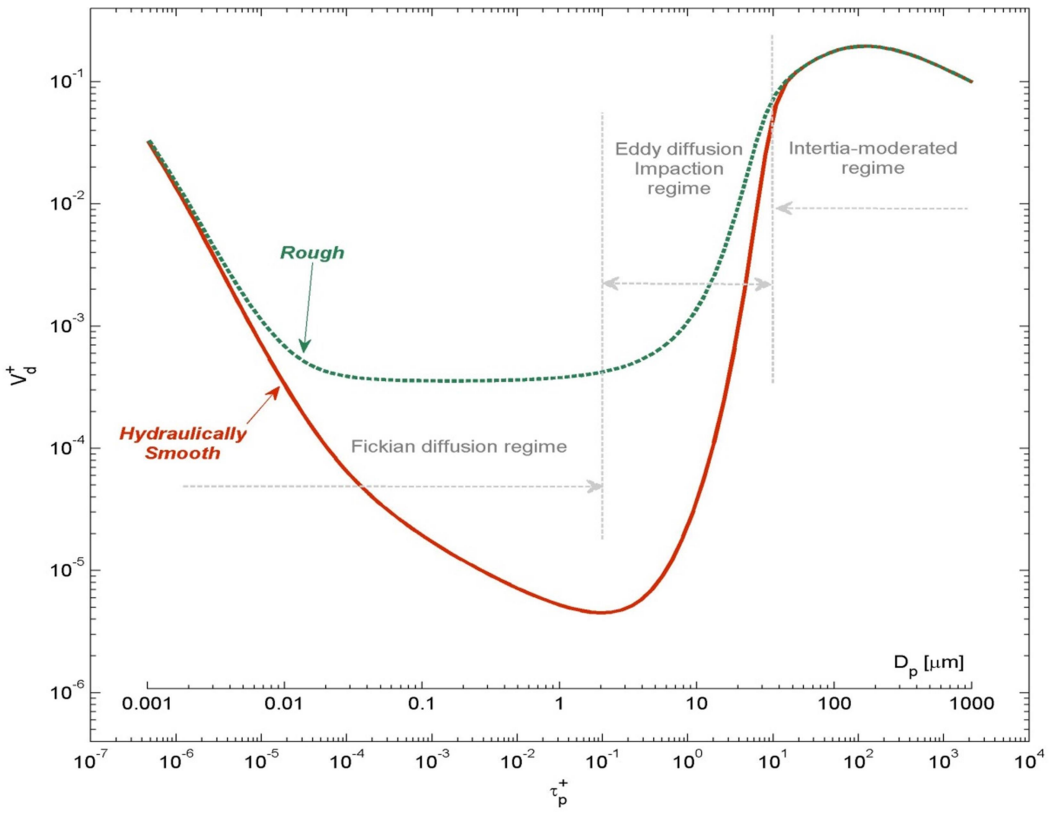

FIG. 2. Universal curve of dimensionless dry deposition velocity (V_d^+) *versus* particle diameter (D_p) or dimensionless particle relaxation time (τ_p^+). This curve represents deposition onto vertical surfaces. *Figure was adopted from Hussein et al. [12].*

Dry deposition mechanism onto a surface is believed to occur through two main stages: First, advection and turbulent mixing that transport suspended particles towards the deposition surface. Second, the particles are transported *via* several mechanisms across the boundary layer, which is a thin layer above the surface. It is believed that the second stage is the one that controls the deposition mechanism when the gas is turbulently well mixed. Guha [2] identified the most important transport mechanisms across the boundary layer as Fickian diffusion, thermophoresis, turbophoresis, electrophoresis and gravitational settling. Saffman lift force, pressure diffusion, stressphoresis and diffusiophoresis are often ignored due to their very small effects compared to other mechanisms, lack of understanding and complications to incorporate them in deposition models. Nowadays, magnetophoresis can have important applications, because it enables to produce magnetic fields higher than before.

As mentioned above, particle size is one of the important parameters needed for calculating V_d. In general, there is a well-known universal dependence of the dimensionless dry deposition velocity (V_d^+) and the dimensionless particle relaxation time (τ_p^+), spaning over 6 orders of magnitude of particle diameter (D_p) and about 9 orders of magnitude of V_d (Fig. 2). Dry deposition is usually considered according to three regimes for V_d curve onto vertical *smooth* surfaces [2, 7, 15, 17, 20]: (1) Turbulent particle diffusion regime ($\tau_p^+ < 1$), (2) Eddy diffusion-impaction regime (τ_p^+ 0.1–10) and (3) Particle inertia-moderated regime ($\tau^+ > 10$). In the first regime, deposition is affected by a combination of Brownian and Eddy diffusion, where V_d is proportional to $Sc^{-2/3}$ and increases with increasing turbulent intensity. The second regime is characterized by a sharp increase of V_d^+ with τ_p^+, where Friedlander and Johnstone [2] and Davis [16] proposed that particles acquire velocities towards the wall due to the turbulent eddies in the turbulent core and buffer layer and then coast across the viscous sublayer because of their inertia. In the third regime, V_d^+ is saturated with τ_p^+ and eventually decreases with increasing τ_p^+ [18, 19].

In this paper, we present a review about the three-layer deposition model with respect to the types of mechanisms and processes and illustrate that with numerical model simulations compared to some empirical observations.

2. Model Development and Description

2.1 Particle Flux across the Boundary Layer

Dry deposition of particles onto surfaces has been of great interest for more than 80 years [1, 21, 22]. There are two main approaches for calculating V_d [2]: Eulerian and Lagrangian. The three-layer deposition model follows an Eulerian approach [3, 4, 11]. The name "three-layer" comes from the fact that in this model, the viscous boundary layer is considered as three sub-layers. Many models have been developed based on three main particle transport mechanisms: Brownian diffusion, turbulent diffusion and gravitational settling. Additionally, some models incorporate other mechanisms, such as thermophoresis, electrostatic drifting, turbophoresis, … etc. [2, 4, 8, 9, 11, 23].

The three-layer dry deposition model is based on the understanding that there is a very thin particle concentration boundary layer within the turbulent boundary layer above a surface. The particle flux, J [$m^{-2}s^{-1}$], across the concentration boundary layer is written in the general form

$$J = J_{Fickian} + J_{Grav} + J_{Turbo} + J_{Ther} + J_{Elec} + J_{Mag} + \sum_n J_n \quad (1)$$

where the terms on the right-hand side respectively represent the particle flux due to Fickian diffusion (Brownian and Eddy), gravitation settling, turpophoresis, thermophoresis, electrophoresis, magnetophoresis and the sum of other weak mechanisms, which can be included in the model formulation if needed. The validity of Eq. (1) has the following assumptions [3]: (a) steady-state particle flux across the boundary layer, one-dimensional and perpendicular to the surface, (b) the particle concentration gradient exists only very close to the deposition surface, (c) there are no sources or sinks of particles within the boundary layer and (d) the surface is a perfect sink for particles.

As illustrated in Fig. 1, the particle reaches a smooth surface – or in other words: hydraulically smooth surface – and gets deposited on it when its center is at height y_0 from the deposition surface. Basically, for spherical particles, this is the radius of the particle (i.e., $y_0 = r_p$). At this height, the particle concentration is zero in the

fluid right above the surface. The concentration boundary layer is assumed to have an upper limit above which particle concentration becomes homogeneous (i.e., $dC/dy = 0$) as a result of the turbulent air mixing [24]. This implies that at the top of the concentration boundary layer (i.e., y_{cbl}) is set at the maximum concentration (i.e., C_∞).

In the case of a rough surface – or in other words: hydraulically rough surface – the concentration boundary layer is shifted away from the surface (i.e., $y_0 = r_p + F$), where F is a function of surface roughness characteristics [12]. It has been confirmed that surface roughness enhances V_d in the particle diffusion regime and the diffusion-impaction regime. In general, topography of a rough surface distorts the air flow characteristics above the surface and the boundary layer itself resulting in a shorter stopping distance of migrated particles towards the surface [2, 3, 13, 14, 25–27]. Many studies relied on the surface roughness formulation based on a single surface property, which is the surface roughness height [5, 7, 11, 28]. However, with this assumption, such dry deposition formulae fail in predicting V_d. Recently, a new approach was provided by Hussein et al. [12] to account for surface roughness based on hybrid parameter (F), which is a combination of surface roughness height (K) and peak-to-peak distance (L) between the roughness elements. In essence, F represents an effective surface roughness length that is used in the assumption for the shift in the concentration boundary layer.

Mathematically, the boundary conditions to solve the particle flux equation are:

$$C\big|_{y=r_p+F} = 0 \quad \text{and} \quad C\big|_{y=y_{cbl}} = 1. \tag{2}$$

Finally, the overall V_d due to all mechanisms included in the particle flux Eq. (1) is simply calculated according to the first assumption at the top of the concentration boundary layer:

$$V_d = \frac{|J|}{C_\infty}. \tag{3}$$

Usually, the particle flux equation is converted into a dimensionless form and then solved. Table 1 lists the nomenclature of each parameter and its conversion into dimensionless form.

Fickian Diffusion

The term “Fickian diffusion” refers to both Brownian diffusion and Eddy diffusion and the particle flux is written as a modified form of Fick’s first law [2]:

$$J_{Fickian} = -\left(\varepsilon_p + D\right)\frac{dC}{dy} \tag{4}$$

where D [m^2 s^{-1}] is Brownian diffusivity and ε_p [m^2 s^{-1}] is Eddy diffusivity of the particle. Contrary to Brownian diffusivity (D), Eddy diffusivity (ε_p) within the boundary layer increases with distance from the surface ($\varepsilon_p = 0$ at the surface) due to the physical constraints imposed by the surface. Therefore, ε_p is a function of the distance from the surface in dimensionless form (y^+) and the air turbulent viscosity (ν_t); see for example Table 2. Typically, the concentration boundary layer is treated as three sublayers when defining the dependence of ε_p on ν_t. This brought the name “three-layer” to the Eulerain approach of the deposition model.

Gravitational Settling

While diffusion is the dominant mechanism for small particles, gravitational settling is the dominant mechanism for big particles. The gravitational settling velocity (V_s) of a particle is the terminal velocity towards the surface [29, 30]:

$$V_s = \left[\frac{4}{3}\frac{gD_p\left(\rho_p - \rho\right)}{\rho C_D}C_c\right]^{\frac{1}{2}} \tag{5}$$

where g [m s^{-2}] is the gravitational acceleration, D_p [m] is the particle diameter, ρ_p [kg m^{-3}] is the particle density, ρ [kg m^{-3}] is the gas density, C_D [--] is the drag coefficient and C_c [--] is the Cunningham slip correction coefficient.

The particle flux due to gravitational settling is simply written as:

$$J_{Grav} = -iV_sC. \tag{6}$$

The deposition surface orientation as vertical, horizontal facing up (floor) or horizontal facing down (ceiling) is presented in the term i as 0, 1 or -1, respectively.

TABLE 1. List of important variables that appeared in the text.

B	Tesla	magnetic field nearby a surface
C	m^{-3}	particle concentration within the boundary layer, in dimensionless form $C^+ = C/C_\infty$
C_∞	m^{-3}	particle concentration above the boundary layer or far away from the surface
C_c	--	Cunningham slip correction coefficient
C_D	--	drag coefficient
C_P	J kg^{-1} K^{-1}	specific heat capacity of air
D	m^2 s^{-1}	Brownian diffusivity of the particle, $D = k_B T C_c / 3\pi\mu D_p$ $D^+ = (\varepsilon_p + D)/\nu$
D_p	m	particle diameter, in dimensionless form $D_p^+ = D_p u^*/\nu$
E	N/C	electric field due to charge accumulation on a surface
e	C	elementary charge of the electron, $e = 1.6\times10^{-19}$ C
g	m s^{-2}	acceleration of gravity
H_{Ther}	--	thermophoretic coefficient by Talbot et al. [33]
J	m^{-2} s^{-1}	total particle flux across the concentration boundary layer towards the surface
J_{Elec}	m^{-2} s^{-1}	particle flux due to electrophoresis, which is caused by electrostatic interaction between the deposited particle and the deposition surface
$J_{Fickian}$	m^{-2} s^{-1}	particle flux due to Brownian and Eddy diffusions
J_{Grav}	m^{-2} s^{-1}	particle flux to gravitational settling
J_{Mag}	m^{-2} s^{-1}	particle flux due to electrophoresis, which is caused by magnetic force exerted on the deposited particle
J_{Ther}	m^{-2} s^{-1}	particle flux due to thermophoresis, which is caused by nearby surface temperature gradients
J_{Turbo}	m^{-2} s^{-1}	particle flux due to turbophoresis, which is caused by inhomogeneous mixing
J_n	m^{-2} s^{-1}	particle flux across the concentration boundary layer due to other mechanisms to be included in the model in the future
K	m	roughness height, in dimensionless form $K^+ = Ku^*/\nu$
K	--	von Karman's constant
K_a	W m^{-2} K^{-1}	thermal conductivity of air
K_p	W m^{-2} K^{-1}	thermal conductivity of the particle
k_B	Joul/K	Boltzmann constant
Kn	--	Knudsen number, $Kn = 2\lambda/D_p$
Sc	--	Schmidt number $Sc = \nu/\rho$
L	m	peak-to-peak distance between roughness elements, in dimensionless form $L^+ = Lu^*/\nu$
m_p	kg	particle mass
n	--	number of elementary charges carried by the particle
Pr	--	Prandtl number of air
Re	--	Reynolds number, $\mathrm{Re} = VD_p/\nu$
r_p	m	particle radius, in dimensionless form $r_p^+ = r_p u^*/\nu$
T	K	absolute temperature
ΔT	K	temperature difference, $T_{air} - T_{surface}$
u^*	m s^{-1}	friction velocity
V_d	m s^{-1}	deposition velocity onto a surface, in dimensionless form $V_d^+ = V_d/u^*$
V_{Elec}	m s^{-1}	migration velocity due to electrophoresis, $V_{Elec}^+ = V_{Elec}/u^*$
V_{Mag}	m s^{-1}	migration velocity due to magnetophoresis, $V_{Mag}^+ = V_{Mag}/u^*$
V_s	m s^{-1}	gravitational settling velocity, in dimensionless form $V_s^+ = V_s/u^*$
V_t	m s^{-1}	migration velocity towards a surface due to turbophoresis, $V_t^+ = V_t/u^*$
V_{Ther}	m s^{-1}	migration velocity due to thermophoresis, $V_{Ther}^+ = V_{Ther}/u^*$

$\langle V'^2_y \rangle$	$m^2\ s^{-2}$	air wall normal fluctuating velocity intensity, in dimensionless form by Guha [2] after Kallio and Reeks [19]: $\langle V'^2_y \rangle^+ = \frac{\langle V'^2_y \rangle}{(u*)^2} = \left[\frac{0.005(y^+)^2}{1+0.002923(y^+)^{2.128}}\right]^2$
$\langle V'^2_{py} \rangle$	$m^2\ s^{-2}$	particle wall normal fluctuating velocity intensity by Johansen [32] (*): $\langle V'^2_{py} \rangle = \langle V'^2_y \rangle \left[1+\frac{\tau_p}{\tau_L}\right]^{-1}$ and in dimensionless form $\langle V'^2_{py} \rangle^+ = \langle V'^2_{py} \rangle / (u*)^2$
y	m	vertical distance from the surface, in dimensionless form $y^+ = yu*/\nu$
y_0	m	distance from the surface at which the particle with a radius r_p is deposited, in dimensionless form $y_0^+ = y_0 u*/\nu$
y_{cbl}	m	depth of the concentration boundary layer above which $dC/dy = 0$ in dimensionless form $y^+_{cbl} = y_{cbl} u*/\nu$
ε_p	$m^2\ s^{-1}$	Eddy diffusivity of the particle, see also Table 2
λ	m	mean free path of air molecules
μ	kg $m^{-1}\ s^{-1}$	dynamic viscosity of the fluid
ν	$m^2\ s^{-1}$	kinematic viscosity of the fluid, $\nu = \mu/\rho$
ν_t	$m^2\ s^{-1}$	air turbulent viscosity, see also Table 2
ρ	kg m^{-3}	fluid density
ρ_p	kg m^{-3}	particle density
σ_t	--	turbulent Schmidt number
τ_L	s	Lagrangian time-scale of the fluid by Johansen [7]: $\tau_L = \nu_t / \langle V'^2_y \rangle$ and in dimensionless form $\tau_L^+ = \tau_L (u*)^2 / \nu$
τ_p	s	particle relaxation time, $\tau_p = m_p C_c / 3\pi\mu D_p$, in dimensionless form $\tau_p^+ = \tau_p (u*)^2 / \nu$

(*) The validity of this expression is limited for $\tau_p^+ < 138$. Most small particles meet this criterion because their $\tau^+_p < 10$; and thus, this formula is reasonable [4].

Turbophoresis

Turbophoresis is a phenomenon that leads to the net migration of particles from regions of high Eddy diffusivity to regions of low Eddy diffusivity [2, 31]. This phenomenon is significant for particles with high inertia suspended in inhomogeneous turbulent fluid. In case of law air speed and small particles, particle momentum is small enough, so that turbophoresis can be neglected.

The particle flux due to this mechanism is written as:

$$J_{Turbo} = V_t C \tag{7}$$

where (V_t) is the deposition velocity due to this mechanism:

$$V_t = -\tau_p \frac{d}{dy} \langle V'^2_{py} \rangle. \tag{8}$$

Here, τ_p [s] is the particle relaxation time:

$$\tau_p = \frac{m_p C_c}{3\pi\mu D_p} \tag{9}$$

where m_p [kg] is the particle mass, C_c [--] is the Cunningham slip correction coefficient, μ [kg $m^{-1}\ s^{-1}$] is the fluid kinematic viscosity and D_p [m] is the particle diameter. $\langle V'^2_{py} \rangle$ is the particle wall normal fluctuating velocity intensity [32]:

$$\langle V'^2_{py} \rangle = \langle V'^2_y \rangle \left[1+\frac{\tau_p}{\tau_L}\right]^{-1} \tag{10}$$

with $\tau_L = \nu_t / \langle V'^2_y \rangle$ as the fluid relaxation time and $\langle V'^2_y \rangle$ is the air wall normal fluctuating velocity intensity, which is adopted in dimensionless form after Kallio and Reeks [19].

TABLE 2. The dependence of the particle Eddy diffusivity (ε_p) on y^+ and ν_t and the dependence of the air turbulent viscosity on (ν_t) on y^+.

$\frac{\varepsilon_p}{\nu} = \left(y^+\right)^{4-\left(y^+\right)^{0.08}} \left[\frac{2.5\times10^7}{\mathrm{Re}}\right]^{\frac{-y^+}{400+y^+}} \times 10^{-3}$	universal expression	Guha [2] after Davies [16]
$\varepsilon_p = \nu_t$	relatively small particles and homogeneous isotropic turbulence	Lai and Nazaroff [3]
$\varepsilon_p = \left[1+\frac{\tau_p}{\tau_L}\right]^{-1} \nu_t$	valid for any particle size (*)	Zhao and Wu [4] after Hinze [44]
$\frac{\nu_t}{\nu} = \begin{cases} \left(\frac{y^+}{14.5}\right)^3, & 0 \le y^+ \le 5 \\ 0.2y^+ + 0.959, & 0 \le y^+ \le 5 \end{cases}$	smooth surfaces	Wood [7] after Lin et al. [45]
$\frac{\nu_t}{\nu} = \begin{cases} 7.67\times10^{-4}\left(y^+\right)^3, & 0 \le y^+ \le 4.3 \\ 10^{-3}\left(y^+\right)^{2.8214}, & 4.3 \le y^+ \le 12.5 \\ 1.07\times10^{-2}\left(y^+\right)^{1.8895}, & 12.5 \le y^+ \le 30 \end{cases}$	smooth surfaces (**)	Lai and Nazaroff [3] after DNS simulation results by Kim et al. [46]
$\frac{\nu_t}{\nu} = \begin{cases} \left(\frac{y^+}{11.15}\right)^3, & 0 \le y^+ \le 3 \\ \left(\frac{y^+}{11.4}\right)^3 - 0.049774, & 3 \le y^+ \le 52.108 \\ 0.4y^+, & 52.108 \le y^+ \end{cases}$	rough surface (***)	Zhao and Wu [11] after parameterization by Johansen [32]

(*) While the Eddy diffusivity is valid for homogeneous turbulent mixing, the expression proposed by Hinze [44] is also valid for inhomogeneous turbulent mixing. This is because the rate-limiting transport mechanisms for particle deposition occur inside the viscous sublayer, which is known to be anisotropic [20], and particles might retain their earlier motion because of inertia into a region that has different turbulence properties.

(**) Lai and Nazaroff [3] also justified that due to the low Brownian diffusivity of particles, the particle concentration boundary layer is generally contained within the viscous sublayer and therefore, the functional dependence of ν_t is most important in the region $0 \le y^+ \le 4.3$. They additionally emphasized that the cube power relationship for this region was observed in simulations and experiments [47–49]. Lai and Nazaroff [3] used the DNS simulation results of Kim et al. [46] and distinguished three sublayers for ν_t/ν.

(***) In general, the above mentioned approaches by Lai and Nazaroff [3] and Zhao and Wu [4] are very similar for $y^+ < 30$ and the only difference is the extension beyond $y^+ = 52.108$ in the Zhao and Wu [4] approach to justify the conditions above a rough surface.

Thermophoresis

Thermophoresis is a phenomenon, where suspended particles in a gas experience a force in the direction opposite to the temperature gradient (∇T) in the fluid nearby a surface [33]. Thermophoresis is of practical importance in many industrial applications (e.g. thermal precipitators). The particle flux due to this mechanism is:

$$J_{Ther} = V_{Ther} C . \tag{11}$$

Here, the thermophoretic velocity is:

$$V_{Ther} = -\frac{C_c \nu H_{Ther}}{T} \frac{dT}{dy} \tag{12}$$

where C_c [--] is the Cunningham slip correction coefficient, ν [m^2 s^{-1}] is the fluid kinematic viscosity, T [K] is the gas temperature,

dT/dy [K m^{-1}] is the temperature gradient above the surface and H_{Ther} is the thermophoretic coefficient:

$$H_{Ther} = \left(\frac{2.34}{1+3.42Kn}\right)\left(\frac{\frac{k_a}{k_p}+2.18Kn}{1+4.36Kn+2\frac{k_a}{k_p}}\right) \quad (13)$$

with k_a and k_p [W m^{-1} K^{-1}] are the thermal conductivities of the air and the particle, respectively. Kn is the Knudsen number.

As suggested by Othmane et al. [34], who used the temperature gradient according to Nerisson [35],

$$\frac{dT}{dy} = \frac{1}{k_a}\frac{\rho C_p u*}{y_0^+ \Pr + \frac{\sigma_t}{\kappa}\ln\left(\frac{y^+}{y_0^+}\right)}\Delta T \quad (14)$$

where Pr = 0.7 is the Prandtl number of air, σ_t = 1 is the turbulent Schmidt number, κ = 0.41 is the von Karman's constant, C_p = 1004 [J kg^{-1} K^{-1}] is the specific heat capacity of air and ΔT (K) is the temperature difference between the top of the boundary layer and the deposition surface. Here, Othmane et al. [34] used y^+ = 500.

Electrophoresis

Electrophoresis is a mechanism, where particles migrate towards a surface due to two mechanisms: (1) electrostatic image forces and (2) electrostatic field due to charge accumulation on the surface [8]. Usually, the effect of charge accumulation (i.e., electrostatic field) is stronger than the effect of image forces. The migration velocity (V_{Elec}) due to the existence of a charged particle in an electric field E [N/C] generated by surface charge accumulation is:

$$V_{Elec} = \frac{neC_cE}{3\pi\mu D_p} \quad (15)$$

where n is the number of elementary charges carried by the particle, e [1.6×10^{-19} C] is the elementary charge of the electron, C_c [--] is the Cunningham slip correction coefficient, μ [kg m^{-1} s^{-1}] is the fluid kinematic viscosity and D_p [m] is the particle diameter.

Magnetophoresis

When a charged particle moves in a magnetic field, it experiences a magnetic force that is proportional to its velocity V [m s^{-1}] and the magnitude of the magnetic field B [Tesla], bearing in mind that the direction of the particle velocity is not parallel (or anti-parallel) to the direction of the magnetic field. The migration velocity (V_{Mag}) due to this mechanism is:

$$V_{Mag} = \frac{neC_c}{3\pi\mu D_p}\vec{V}\times\vec{B} \quad (16)$$

where n is the number of elementary charges carried by the particle, e [1.6×10^{-19} C] is the elementary charge of the electron, C_c [--] is the Cunningham slip correction coefficient, μ [kg m^{-1} s^{-1}] is the fluid kinematic viscosity and D_p [m] is the particle diameter.

2.2 Numerical Solution for the Particle Flux Equation

More conveniently, the deposition velocity is derived in dimensionless formulation for Eq. (1):

$$\frac{dC^+}{dy^+}+\frac{1}{D^+}\left[V_{Mag}^+ + V_{Elec}^+ + V_{Ther}^+ + iV_s^+ + \tau_p^+\frac{d}{dy^+}\left\langle V'^2_{py}\right\rangle^+\right]C^+ = \frac{V_d^+}{D^+} \quad (17)$$

and here, the + superscript denotes that the variable is in dimensionless form (Table 1).

The general solution for C^+ as a function of y^+ is [36]:

$$C^+ = \frac{1}{F\left(y^+\right)}\int_{y_0^+}^{y^+}\frac{V_d^+}{D^+}F(x)\cdot dx \quad (18)$$

where

$$F(x) = \exp\left(\int_{y_0^+}^{x} p\left(y^+\right)\cdot dy^+\right) \quad (19)$$

$$p\left(y^+\right) = \frac{1}{D^+}\left[V_{Mag}^+ + V_{Elec}^+ + V_{Ther}^+ + iV_s^+ + \tau_p^+\frac{d}{dy^+}\left\langle V'^2_{py}\right\rangle^+\right] \quad (20)$$

and the integrations are evaluated across the concentration boundary layer. In other words, the boundary conditions for this first-order differential Eq. (18) are:

$$C^+\Big|_{y^+=y_0^+=r_p^++F^+} = 0 \quad \text{and} \quad C^+\Big|_{y^+=y_{cbl}^+} = 1. \quad (21)$$

Substituting the first boundary condition into the general solution, Eq. (19) is already satisfied, because the particle concentration at the surface is null. The second boundary condition yields the deposition velocity:

$$\frac{1}{V_d^+} = \frac{1}{F\left(y_{cbl}^+\right)} \int_{y_0^+}^{y_{cbl}^+} \frac{1}{D^+} F(x) \cdot dx \qquad (22)$$

3. Model Simulations

3.1 Smooth Surface

In this section, several model simulations were made to illustrate the effect of different dry deposition mechanisms. In the first place, the model simulation was made for the diffusion mechanisms and then gravitational settling was included after showing the effect of turbophoresis. Then, three weak mechanisms were considered: thermophoresis, electrophoresis and magnetophoresis. All model simulations were made to calculate the dry deposition velocity towards smooth surfaces. For universality, all model simulations are presented in dimensionless form; i.e., dimensionless dry deposition velocity (V_d^+) and dimensionless particle relaxation time (τ_p^+).

Brownian and Eddy Diffusion (Fickian Diffusion)

Initially, the effect of Brownian diffusion was assessed by assuming three heights (y_{cbl}^+ = *30, 100 and 300*) for the concentration boundary layer (Fig. 3). In general, the height of the concentration boundary layer defines the concentration gradient, because the particle concentration in the fluid right above the surface (i.e., $C = 0$ at $y^+ = r_p^+$) is assumed to be null, but it increases to reach a steady-state value (C_∞ *at* y_{cbl}^+) at the top of the concentration boundary layer. Therefore, the higher the concentration boundary layer is, the less is the concentration gradient. As can be seen from the model simulation (Fig. 3), V_d^+ increases with increasing the concentration gradient (i.e., with decreasing the height of the concentration boundary layer). It is also higher for smaller particles (i.e., shorter relaxation time of the particle τ_p^+). In other words, V_d^+ is enhanced by one order of magnitude when the concentration boundary layer height is decreased by one order of magnitude. It is also enhanced by five orders of magnitude when τ_p^+ is decreased by three orders of magnitude.

The Brownian diffusion occurs regardless of the fluid turbulence state. Once the fluid is stirred (i.e., turbulent fluid), the effect of Eddy diffusion starts to happen. This effect is illustrated in Fig. 3 by assuming a friction velocity u^* = 0.1 m/s. The higher the u^* is, the higher is the turbulence in the fluid. The enhancement in V_d^+ is seen for all particles. The overall effect of the Brownian and Eddy diffusion (i.e., Fickian diffusion) is summarized with famous U-shape of the dependence of V_d^+ on τ_p^+.

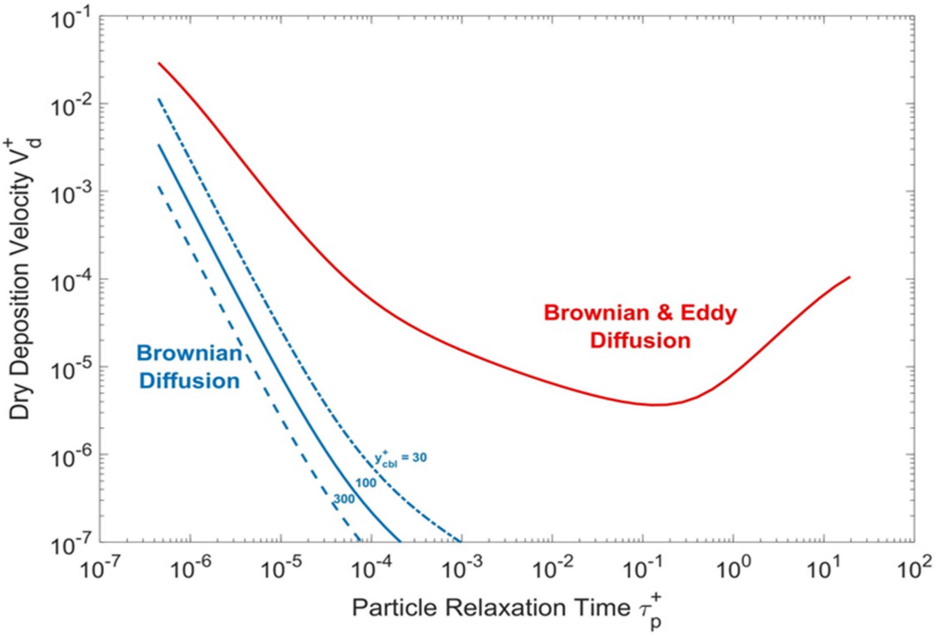

FIG. 3. Dimensionless dry deposition velocity (V_d^+) *versus* dimensionless particle relaxation time (τ_p^+) illustrating the effect of Brownian diffusion (three depths of the concentration boundary layer) compared to the model calculations by including Eddy diffusion. *The model calculations were made for a vertical surface at standard air conditions* ($T = 21\ ^oC$ *and* $P = 1$ *atm*), *friction velocity* $u^* = 0.1$ *m/s and spherical particles with unit density (i.e.,* $\rho_p = 1$ *g/cc*).

Turbophoresis

In practice, fluid turbulance can be inhomogeneous. As postulated in the "model development and description", turbophoresis becomes significant for large particles in the conditions of inhomogeneous turbulence missing in the fluid. This is illustrated in Fig. 4, where four model simulations were made. The first model simulation was made for Fickian diffusion at $u^* = 0.1$ *m/s* without turbophoresis effect included (back curve in Fig. 4). That was compared to three model simulations by including the effect of turbophoresis with three values of $u^* = 0.01$, 0.1 and 1 m/s (red curves in Fig. 4). As clearly seen, the U-shape of V_d^+ *versus* τ_p^+ is more pronounced, now enhancing V_d^+ with a couple of orders of magnitude for large particles (i.e., long relaxation time of the particle τ_p^+). For small particles (i.e., short relaxation time of the particle τ_p^+), V_d^+ is also enhanced by several orders of magnitude when u^* is increased by one order of magnitude.

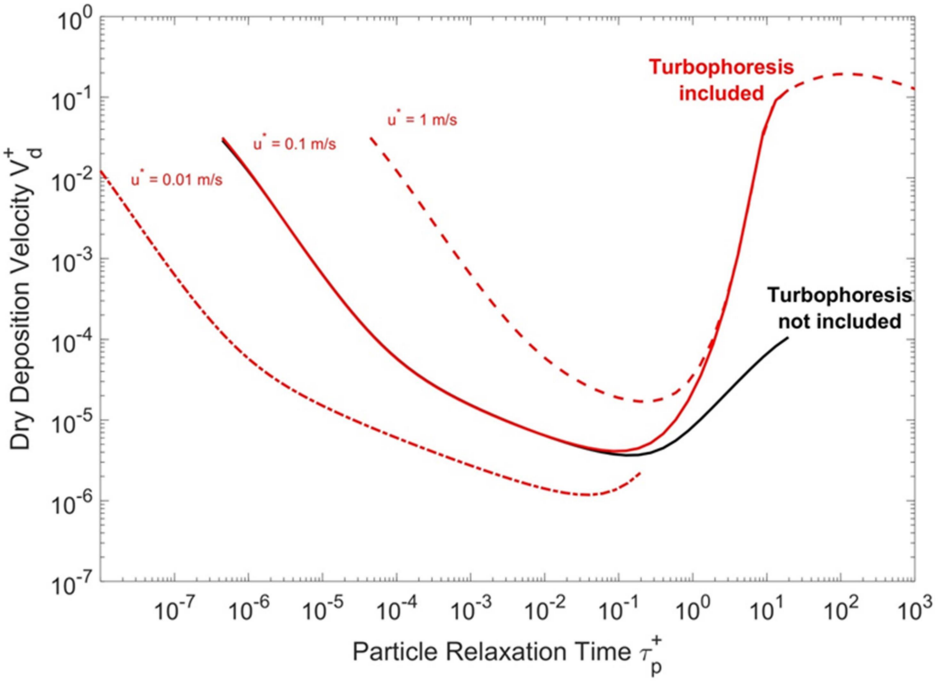

FIG. 4. Dimensionless dry deposition velocity (V_d^+) *versus* dimensionless particle relaxation time (τ_p^+) illustrating the effect of turbophoresis at three friction velocity (u^*) values. *The model calculations were made for a vertical surface at standard air conditions* ($T = 21\ ^oC$ *and* $P = 1$ *atm*) *and spherical particles with unit density (i.e.,* $\rho_p = 1000\ kg/m^3$).

In fact, the inclusion of turbophoresis was a critical step towards explaining the high empirical values of V_d^+ towards vertical surfaces. Hence, the well-known universal dependence of the V_d^+ on τ_p^+ was not possible without this important development (i.e., inclusion of turbophoresis) in three-layer models. As postulated before, there can be distinguished three regimes for V_d curve onto vertical *smooth* surfaces: turbulent particle diffusion regime ($\tau_p^+ < 1$), Eddy diffusion-impaction regime (τ_p^+ 0.1–10) and particle inertia-moderated regime ($\tau^+ > 10$). The Brownian and Eddy diffusion perfectly explains the dependence of V_d^+ on τ_p^+ within the first regime, whereas turbophoresis explains the sharp increase of V_d^+ with τ_p^+ within the second regime. Within the third regime, V_d^+ is saturated with τ_p^+ and eventually decreases with increasing τ_p^+.

Gravitational Settling

This mechanism is important whenever the deposition surface is not vertical. While moving inside the fluid, the forces acting on the particle are: force of gravity, drag force opposite to the direction of motion and buoyant force making the particle float in the fluid, when its density is less than the density of the fluid. The particle reaches its terminal velocity when the resultant force from all external forces is null; i.e., the particle acceleration is zero and its speed is constant.

Eq. (5) was derived according to the terminal velocity conditions. Its direction is always downwards. For a surface that is horizontal and facing up (e.g. a floor), the gravitational settling is towards the surface in a direction parallel with the effect of Fickian and turbophoresis mechanisms; i.e., V_d^+ is increased (Fig. 5). For a horizontal surface facing down (e.g. a ceiling), the gravitation settling is away from the surface in a direction antiparallel with the effect of Fickian and turbophoresis mechanisms; i.e., V_d^+ is decreased (Fig. 6). For a surface that is inclined with an angle, the scalar product between the direction of the settling velocity and the normal to the surface needs to be taken into account.

As can be seen for the model simulations (Figs. 5 and 6), V_d^+ increases with τ_p^+, because the larger the particle is, the more massive is the particle. For a 2 μm particle diameter ($\tau_p^+ = 0.1$), V_d^+ on a horizontal facing up surface is increased by four orders of magnitude when compared to deposition on a vertical surface (Fig. 5). One order of magnitude change in the particle density results in V_d^+ increasing by one order of magnitude.

Thermophoresis

This mechanism is usually well observed on the walls nearby heaters, where particles are deposited on the walls due to the high air temperature and cold wall; i.e., temperature gradient towards the wall forces particle to migrate towards the wall. This mechanism is also utilized in air purifiers, where the air stream is heated to generate a temperature gradient to force air pollution to migrate towards collection surfaces as a method to clean indoor air.

Fig. 7 illustrates the effect of thermophoresis on V_d^+ for two temperature differences in either directions towards and away from a vertical surface. This mechanism has its significant effect within the particle diameter range, where neither diffusion nor inertial forces are significant; i.e., τ_p^+ in the range 0.001–0.1 (or in other words D_p in the range 0.1–1 μm).

Electrophoresis

This mechanism has a wide range of applications, such as in agriculture, industry, materials science, medical sciences, … etc. Simply, a charge accumulation on a surface will force particles with a certain charge to either get an enhanced deposition or *vice versa*. For example, a certain type of matter can be deposited in patterns as thin films on substrates by creating a charge pattern that attracts the particles and make them deposit efficiently in the wanted pattern. Fig. 8 illustrates the effect of electrophoresis on V_d^+ for two values of nearby-surface electric field. This mechanism has its significant effect for submicron particles ($D_p < 1$ μm).

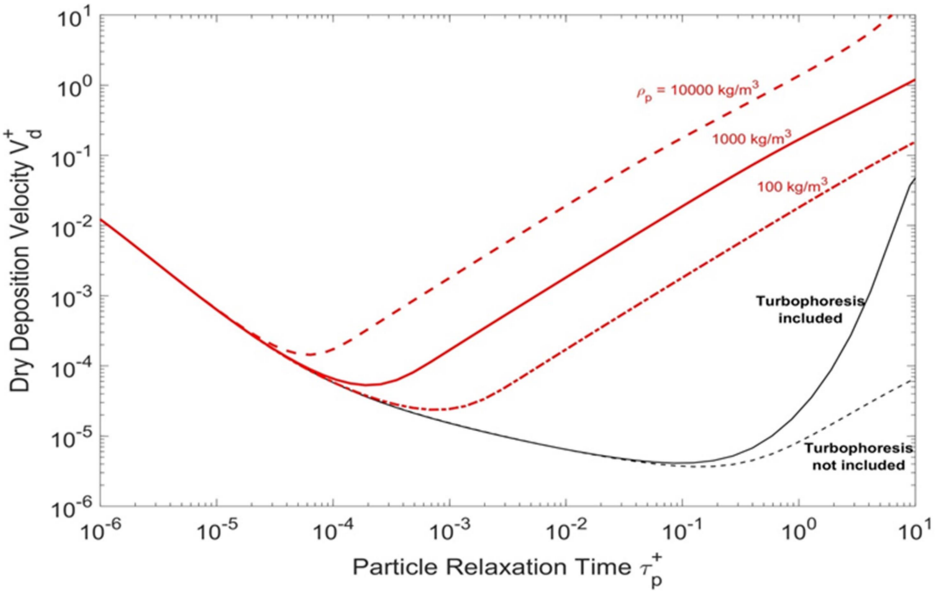

FIG. 5. Dimensionless dry deposition velocity (V_d^+) *versus* particle relaxation time (τ_p^+) illustrating the effect of gravitational settling for three densities (ρ_p) and compared to two models without including gravitational settling (black curves, ρ_p = *1000 kg/m^3*). *The model calculations were made for a vertical surface (black curves) and horizontal facing up surfaces (red curves) at standard air conditions* (T = *21 °C and* P = *1 atm*).

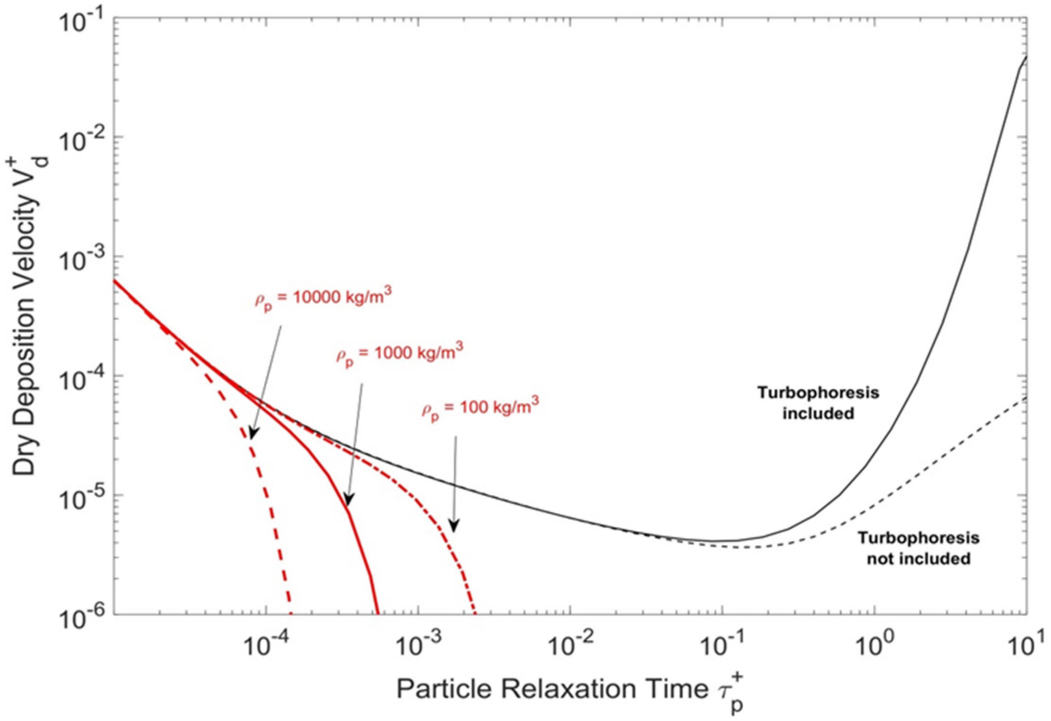

FIG. 6. Dimensionless dry deposition velocity (V_d^+) *versus* dimensionless particle relaxation time (τ_p^+) illustrating the effect of gravitational settling for three particle densities (ρ_p) and compared to two other models without including gravitational settling (black curves, ρ_p = *1000 kg/m^3*). *The model calculations were made for a vertical surface (black curves) and horizontal facing down surfaces (red curves) at standard air conditions* (T = *21 ^{o}C and* P = *1 atm*).

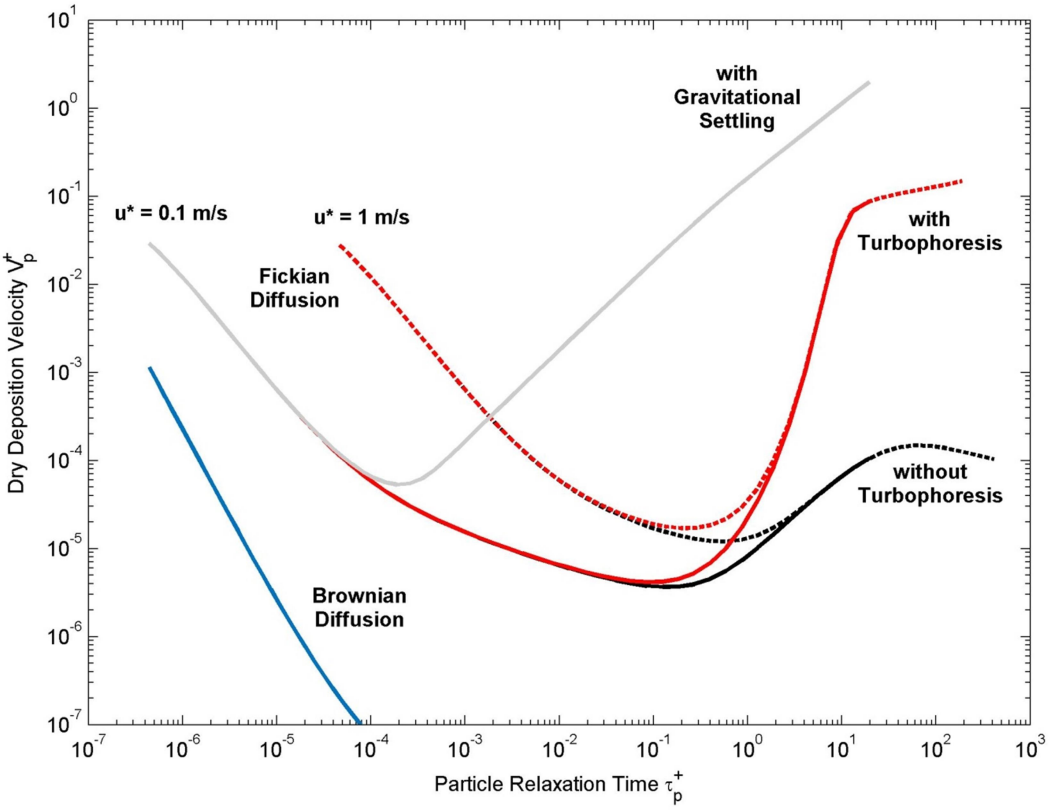

FIG. 7. Model simulations showing the difference between the main processes included in three-layer deposition models. *The model calculations were made for a vertical surface (all curves except for the gray curve, which was made for a horizontal facing up surface) at standard air conditions* (T = *21 ^{o}C and* P = *1 atm*) *and spherical particles with unit density (i.e.,* ρ_p = *1000 kg/m^3*).

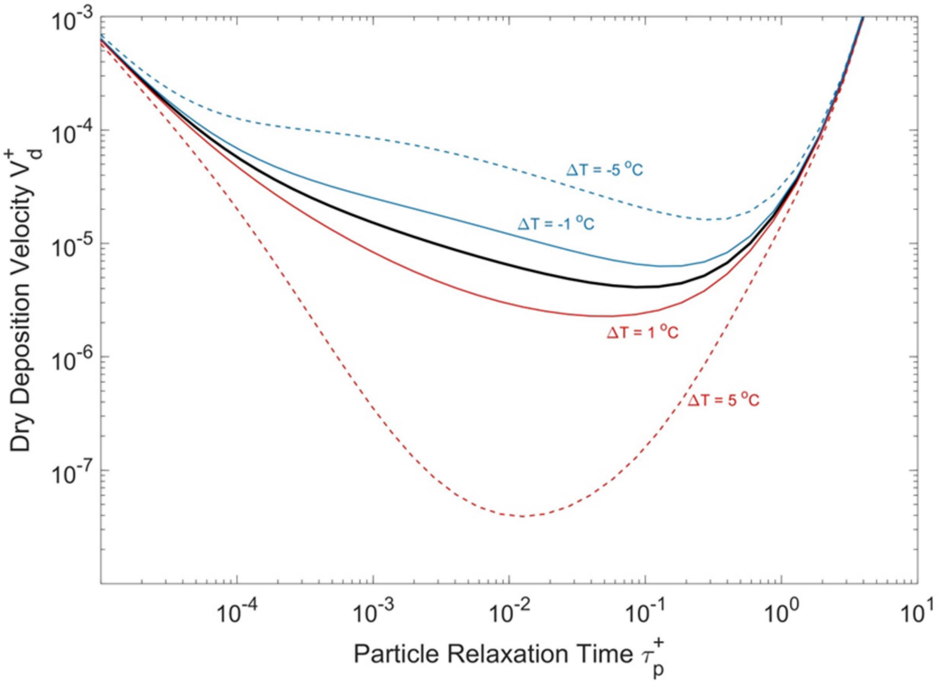

FIG. 8. Dimensionless dry deposition velocity (V_d^+) *versus* dimensionless particle relaxation time (τ_p^+) illustrating the effect of thermophoresis with two different temperature gradients causing thermophoresis migration parallel (blue curves) or antiparallel (red curves) with the effect of Fickian diffusion mechanism. *The model calculations were made for a vertical surface at standard air conditions* (T = 21 °C *and* P = 1 *atm*), *friction velocity* u^* = 0.1 *m/s and spherical particles with unit density (i.e.,* ρ_p = 1000 *kg/m*^{3}).

Magnetophoresis

This mechanism has not been very popular, because it requires a strong magnetic field to have significant effects. In the near future and with the help of advanced technology to generate magnetic fields with high intensity, this mechanism might have important applications in the field of materials science and the development of thin films and nanotechnology.

Fig. 9 illustrates the effect of magnetophoresis on V_d^+ for two magnetic field intensities to migrate particles in either directions towards and away from a vertical surface. This mechanism has its significant effect for nanoparticles (D_p < 40 nm); the smaller the particles are, the more significant is the effect of this mechanism.

As an overall comparison between different processes, Figure 10 illustrates them on the same plot.

Rough Surface

In practice, surfaces are not ideally smooth. To be more specific, surfaces are not hydraulically smooth. This is an important fact when dealing with environmental surfaces for the purpose of estimating particle losses. The surface roughness of environmental surfaces can vary from a couple of microns to several millimeters. Fig. 11 illustrates the effect of surface roughness (summarized by F^+) on V_d^+ for an ordinary rough surface (F^+ = 0.1) and an extremely rough surface (F^+ = 1). The surface roughness affects a wide range of particle sizes including submicron and micron particles.

3.1 Comparison with Empirical Data

In practice, the evaluation of the model calculations against experimental observations is not solely made for a certain process. For example, the Fickian diffusion can't be neglected. To start with, let us consider the experimental data made by Liu and Agarwal [18] to empirically determine the particle deposition inside vertical glass tubes (Fig. 12). This is considered a benchmark for dry deposition model calculations for spherical particles (ρ_p = 0.92 g/cm^3, τ_p^+ = 0.21–774) deposited on vertical surfaces. Later, El-Shobakshy [37] repeated this experiment by taking into consideration spherical particles (ρ_p = 1.5 g/cm^3, τ_p^+ = 0.1–10) deposited inside vertical tubes made of glass or brass (Fig. 12).

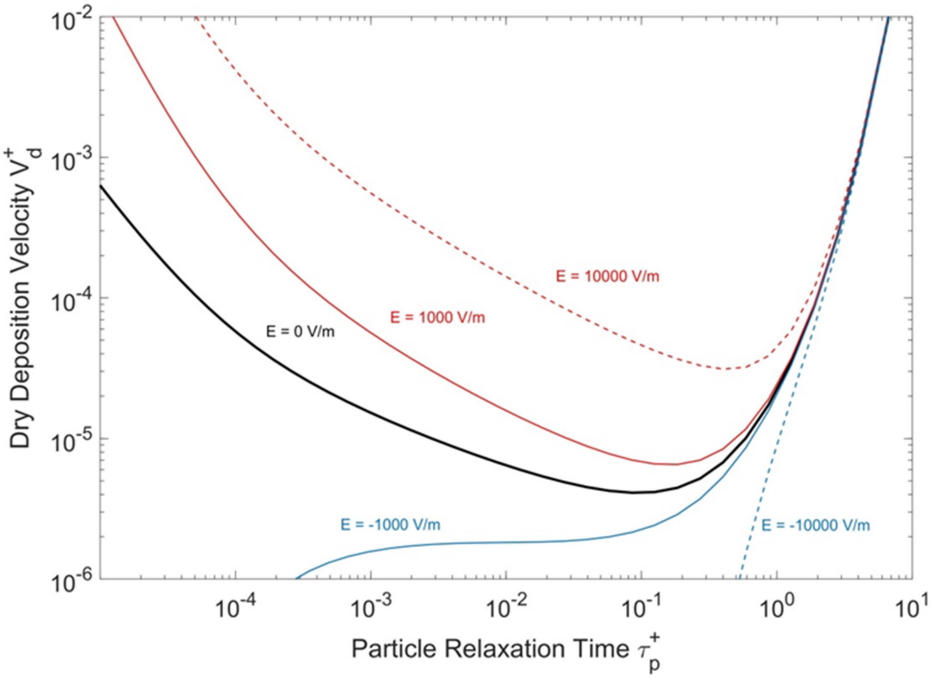

FIG. 9. Dimensionless dry deposition velocity (V_d^+) *versus* dimensionless particle relaxation time (τ_p^+) illustrating the effect of electrophoresis with two different electrostatic field strengths causing electrostatic drifting parallel (red curves) or antiparallel (blue curves) with the effect of Fickian diffusion mechanism. *The model calculations were made for a vertical surface at standard air conditions* ($T = 21\ ^oC$ *and* $P = 1$ *atm*), *friction velocity* $u^* = 0.1$ *m/s and spherical particles with unit density (i.e.,* $\rho_p = 1000\ kg/m^3$) *carrying a negative charge* (*-3e*).

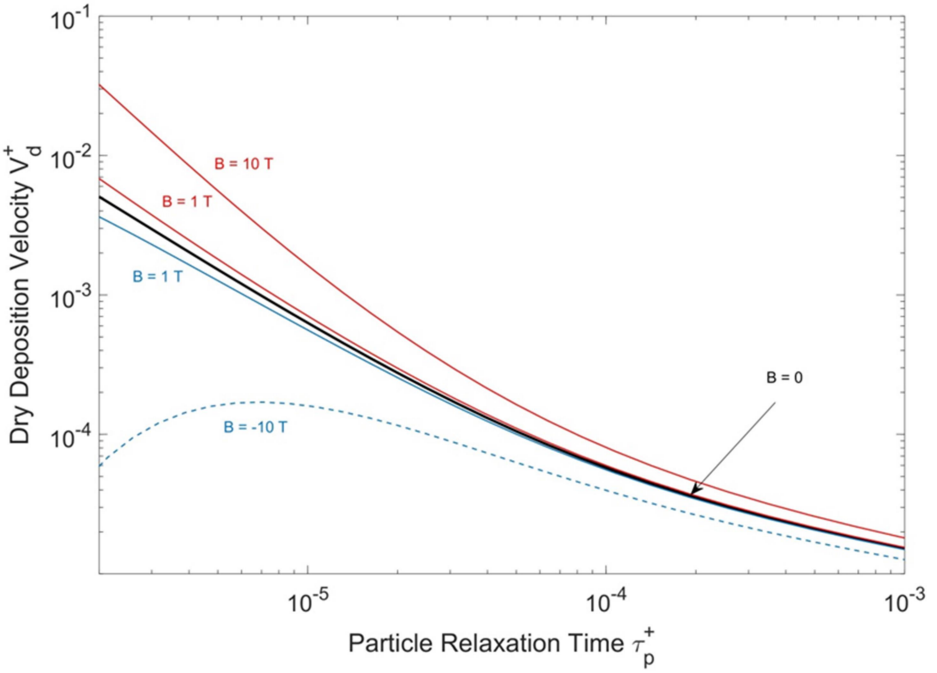

FIG. 10. Dimensionless dry deposition velocity (V_d^+) *versus* dimensionless particle relaxation time (τ_p^+) illustrating the effect of magnetophoresis with two different magnetic field strengths causing electrostatic drifting parallel (red curves) or antiparallel (blue curves) with the effect of Fickian diffusion mechanism. *The model calculations were made for a vertical surface at standard air conditions* ($T = 21\ ^oC$ *and* $P = 1$ *atm*), *friction velocity* $u^* = 0.1$ *m/s and spherical particles with unit density (i.e.,* $\rho_p = 1000\ kg/m^3$) *carrying a negative charge* (*-3e*) *and having a velocity component* ($v_0 = 10$ *m/s) parallel to the surface*.

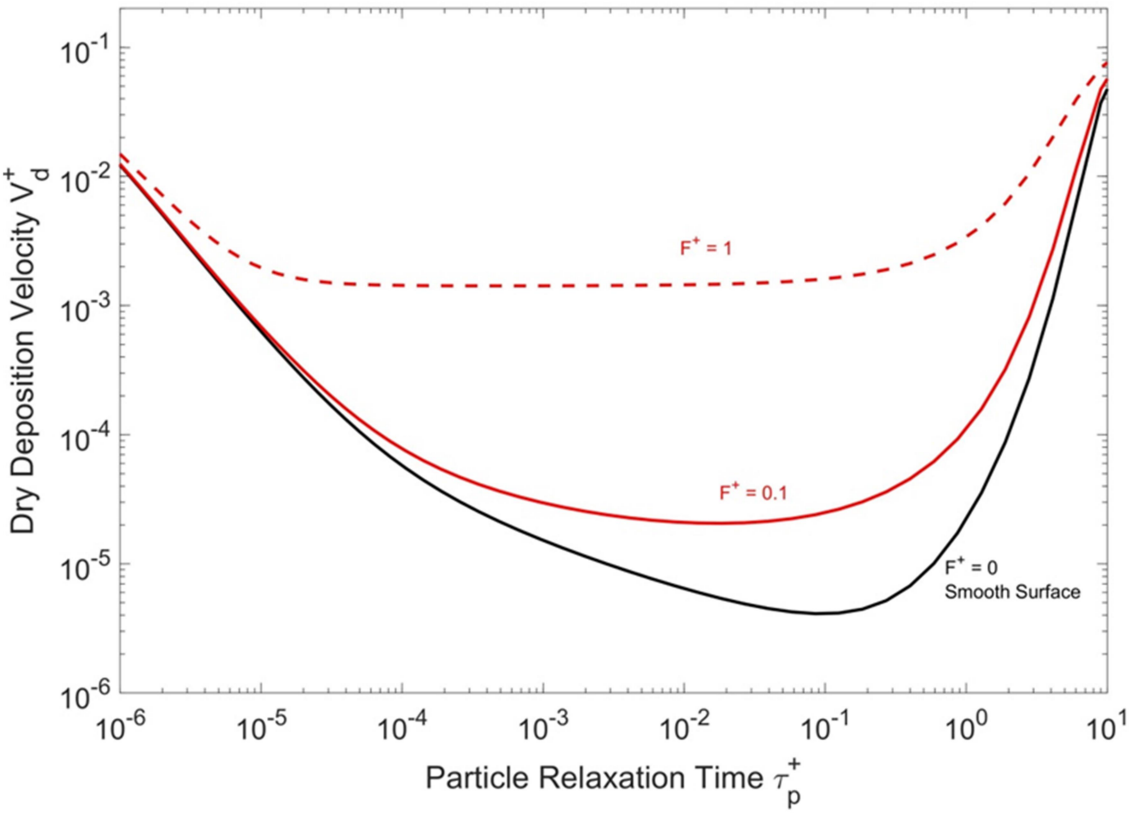

FIG. 11. Dimensionless dry deposition velocity (V_d^+) *versus* dimensionless particle relaxation time (τ_p^+) illustrating the effect of surface roughness. *The model calculations were made at standard air conditions* (*T = 21 °C and P = 1 atm*), *friction velocity u* = 0.1 m/s and spherical particles with unit density (i.e., ρ_p = 1000 kg/m^3*).

The dry deposition model calculations for V_d^+ compare well with the empirical data provided by both Liu and Agarwal [18] and El-Shobakshy [37]. It is presumed that glass is smooth, but in practice, it is not. The model calculations showed a deviation from the empirical data when considering that the vertical glass tubes are smooth; therefore, a surface roughness parameter F^+ = 0.2 was needed to match the model calculations with the empirical data. As for the brass surfaces reported by El-Shobakshy [37], the surface roughness parameter was needed to be F^+ = 1 and 3. The surface roughness height provided by El-Shobakshy [37] was K^+ = 0.56 and 1.65. As mentioned before, when introducing F^+ parameter, it describes the surface roughness based on the mean surface roughness height (K^+) and the mean inter-distance between roughness elements (L^+). This description is more comprehensive than just taking the surface roughness height (K^+) alone into account.

Before trying model evaluation against environmental surfaces, we shall consider the simplest case reported by Sehmel [38], which was the deposition of spherical particles (ρ_p = 1.5 g/cm^3, τ_p^+ = 0.005–40) on a horizontal smooth surface setup in a wind tunnel (Fig. 13). Since the surfaces were smooth, we used F^+ = 0 in the model calculations and the result agrees well with the empirical data.

Slinn [39] reviewed the deposition of spherical particles (ρ_p = 1.5 g/cm^3) on rough surfaces: artificial grass, gravel, water and grass [38, 40–42] with friction velocity u^* = 19, 22, 40 and 36 cm/s, respectively (Fig. 14). The model calculation was made by using F^+ ~0.5 for gravel, water and grass, whereas F^+ ~1.6 was assumed for artificial grass. Fig. 15 also presents additional model calculations compared to spherical particle deposition on artificial grass reported by Chamberlain [43]. In fact, the model calculations can be extended to reproduce particle deposition on many vegetation types (Fig. 16).

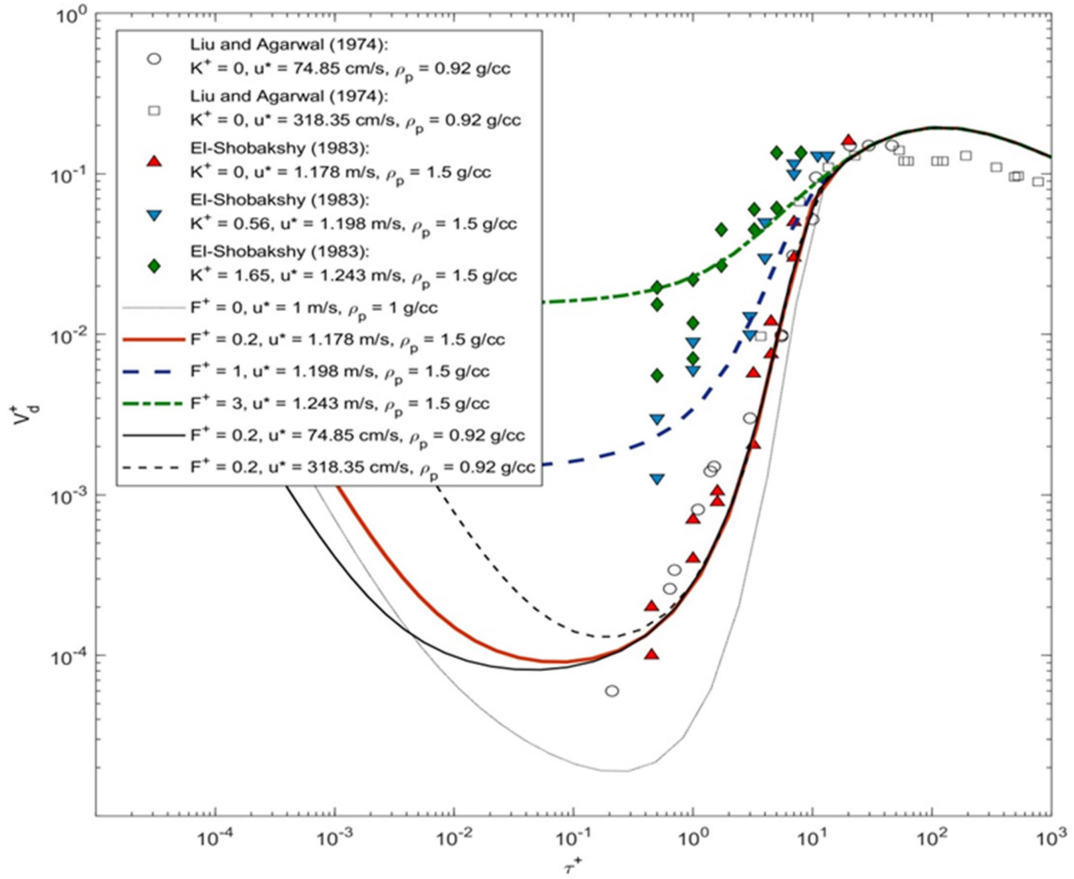

FIG. 12. Dry deposition velocity model calculations compared to empirical data observed for spherical particles deposited inside vertical tubes (glass or brass) as reported by Liu and Agarwal [18] and El-Shobakshy [37].

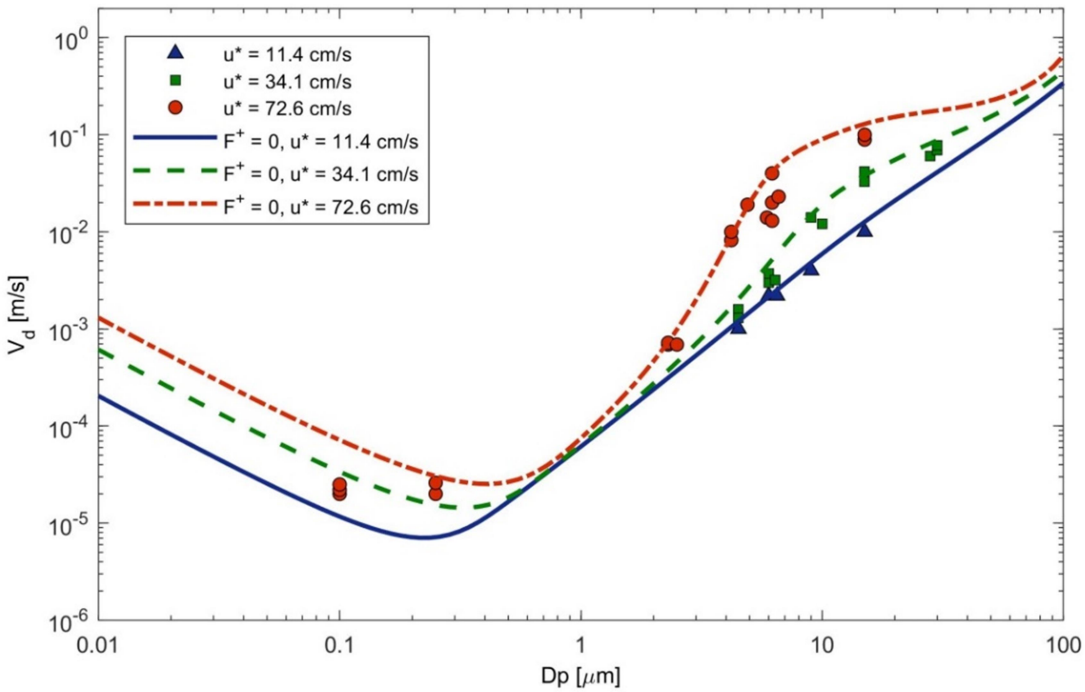

FIG. 13. Dry deposition velocity model calculations compared to empirical data observed for spherical particle (ρ_p = 1.5 g/cm^3) deposition onto horizontal smooth surfaces as reported by Sehmel [38].

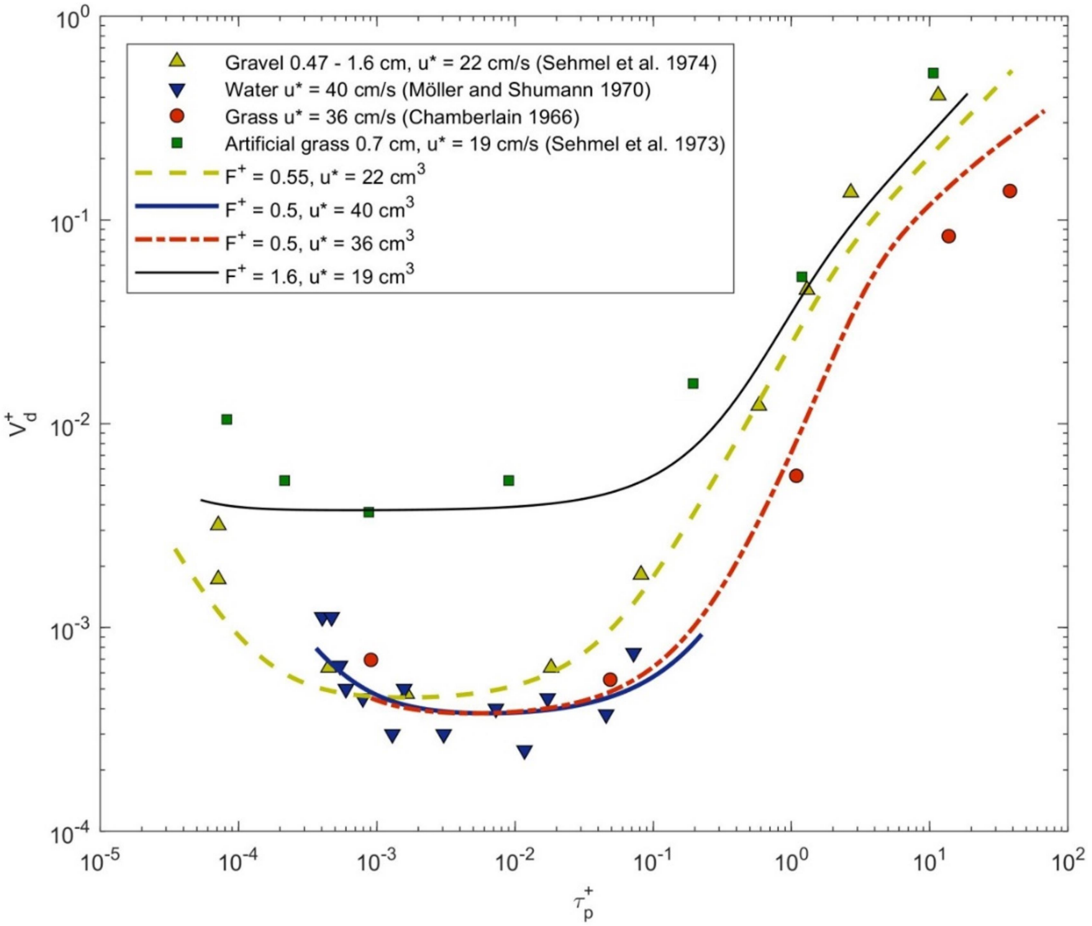

FIG. 14. Dry deposition velocity model calculations compared to empirical data observed for spherical particle (ρ_p = 1.5 g/cm^3) deposition onto horizontal rough surfaces: grass [42], artificial grass [38], gravel [40] and water [41].

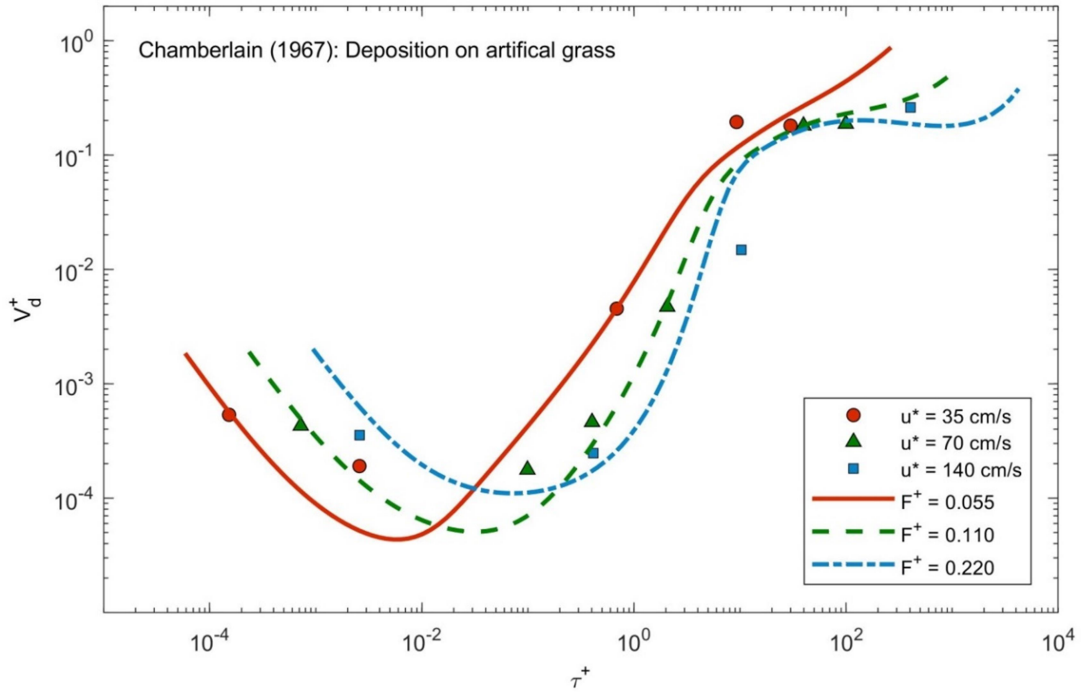

FIG. 15. Dry deposition velocity model calculations compared to empirical data observed for spherical particle (ρ_p = 1.5 g/cm^3) deposition onto horizontal rough surfaces of artificial grass [43].

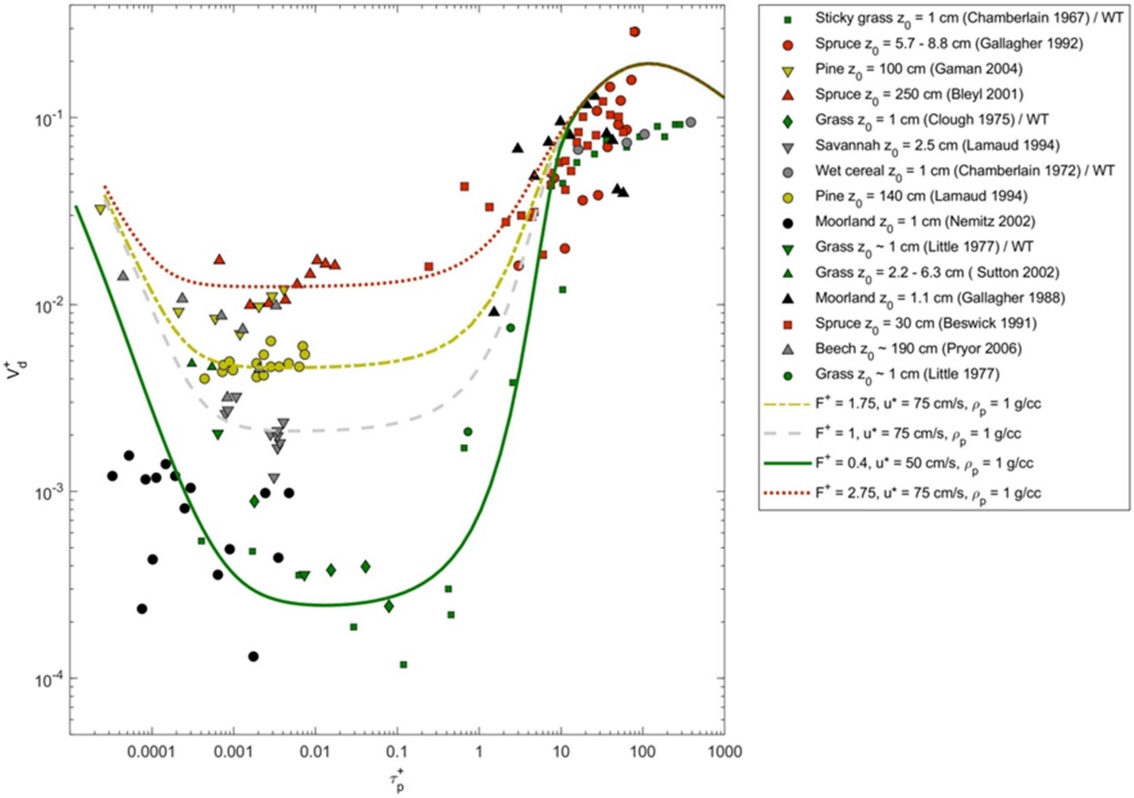

FIG. 16. Dry deposition velocity model calculations compared to empirical data observed for deposition onto different types of vegetation [50–62].

4. Summary and Conclusions

The development of dry deposition modelling is dated back to the early era of the 20th century. Meanwhile, several experimental setups emerged to fulfill the need of testing the performance of model approaches; that was clearly seen in the literature published in the beginning of the 1960s and until the end of the 1980s. During the past twenty years, the model accuracy was significantly enhanced in line with the development of more precise experimental setups and the introduction of advanced technologies. To the date, dry deposition models are capable of simulating particle deposition on a vast range of surfaces and have been used in many applications, such as atmospheric climate and air quality models, industrial processes, nanomaterials, clean rooms, building engineering, particle losses inside sampling lines, health effect of atmospheric particles and pharmaceutics.

In this paper, we presented the basic concepts that have been developed and implemented in dry deposition models and illustrated the effect of different processes on the transport rate of suspended particles in the fluids towards surfaces. As a benchmark for the accuracy of the current dry deposition modelling, we presented a comparison between model calculations and experimental data-bases found in the literature. As a main conclusion, the current dry deposition models are capable of accurately predicting the dry deposition velocities onto almost any surface type and can cover a wide range of particle size (diameter 0.001–100 μm). However, additional research is needed to further develop the current model concepts, so that they include other processes that have specific industrial applications. It is also very important to develop the experimental setup of dry deposition measurements by implementing state-of-the-art technology. For instance, investigations on extreme surface conditions and fluid characteristics are also valuable.

Acknowledgments

The authors would like to acknowledge Prof. Laila Abu-Hassan for her precious advice and encouragement for preparing this review.

References

[1] Corner, J. and Pendlebury, E.D., Proceedings Phys. Soc., B64 (1951) 645.

[2] Guha, A., J. Aerosol Sci., 28 (1997) 1517.

[3] Lai, A.C.K. and Nazaroff, W.W., J. Aerosol Sci., 31 (2000) 463.

[4] Zhao, B. and Wu, J., Atmos. Environ., 40 (2006) 457.

[5] Browne, L.W.B., Atmos. Environ., 8 (1974) 801.

[6] Wan, S.G., Chinese Sci. Bull., 26 (1981) 1145.

[7] Wood, N.B., J. Aerosol Sci., 12 (1980) 275.

[8] McMurry, P.H. and Rader, D. J., Aerosol Sci. Technol., 4 (1985) 249.

[9] Nazaroff, W.W. and Cass, G.R., Environ. Intern., 15 (1989) 567.

[10] Lai, A.C.K., Atmos. Environ., 39 (2005) 3823.

[11] Zhao, B. and Wu, J., Atmos. Environ., 40 (2006) 6918.

[12] Hussein, T., Kubincová, L., Dohányosová, P., Hruška, A., Džumbová, L., Hemerka, J., Kulmala, M. and Smolik, J., Build. Environ., 44 (2009) 2056.

[13] Hussein, T., Hruška, A., Dohányosová, P., Džumbová, L., Hemerka, J., Kulmala, M. and Smolik, J., Atmos. Environ., 43 (2009) 905.

[14] Hussein, T., Smolik, J., Kerminen, V.-M. and Kulmala, M., Aerosol Sci. Technol., 46 (2012) 44.

[15] Friedlander, S.K. and Johnstone, H.F., Ind. Engng. Chem., 40 (1957) 1151.

[16] Davies, C.N., "Aerosol Science", (Academic Press, London, 1966).

[17] Gardner, G.C., Int. J. Multiphase Flow, 2 (1975) 213.

[18] Liu, B.Y.H. and Agarwal, J.K., J. Aerosol Sci., 5 (1974) 145.

[19] Kallio, G.A. and Reeks, M.W., Int. J. Multiphase Flow, 15 (1989) 433.

[20] Young, J.A., J. Fluid Mech., 340 (1997) 129.

[21] Millikan, R.A., Phys. Rev., 22 (1923) 1.

[22] Langstroth, G.O. and Gillespie, T., Canad. J. Res., B25 (1947) 455.

[23] Crump, J.G., Flagan, R.C. and Seinfeld, J.H., Aerosol Sci. Technol., 2 (1983) 303.

[24] Bejan, A., "Convection Heat Transfer", 2nd Ed., (Wiley, New York, 1995).

[25] Fogh, C.L., Byrne, M.A., Roed, J. and Goddard, A.J.H., Atmos. Environ., 31 (1997) 2193.

[26] Abadie, M., Limam, K. and Allard, F., Build. Environ., 36 (2001) 821.

[27] Thatcher, T.L., Lai, A.C.K., Moreno-Jackson, R., Sextro, R.G. and Nazaroff, W.W., Atmos. Environ., 36 (2002) 1811.

[28] Sippola, M.R. and Nazaroff, W.W., Aerosol Sci. Technol., 38 (2004) 914.

[29] Seinfeld, J.H. and Pandis, S.N., "Atmospheric Chemistry and Physics", (Wiley, New York, 1998).

[30] Hinds, W.C., "Aerosol Technology: Properties, Behavior and Measurement of Airborne Particles", (Wiley, New York, 1999).

[31] Reeks, M.W., J. Aerosol Sci., 14, (1983) 729.

[32] Johansen, S.T., Int. J. Multiphase Flow, 17 (1991) 355.

[33] Talbot, L., Cheng, R.K., Schefer, R.W. and Willis, D.R., J. Fluid Mech., 101 (1980) 737.

[34] Othmane, M.B., Havet, M., Gehin, E., Solliec, C. and Arroyo, G., J. Food Eng., 105 (2011) 400.

[35] Nerisson, P., Ph.D. Thesis, University of Toulouse, France, (2009).

[36] Boyce, W.E. and DiPrima, R.C., "Elementary Differential Equations and Boundary Value Problems", 2nd Ed., (John Wiley & Sons, Canada, 1992).

[37] El-Shobokshy, M.S., Atmos. Environ., 17 (1983) 639.

[38] Sehmel, G.A., J. Aerosol Sci., 4 (1973) 125.

[39] Slinn, W.G.N., Nuclear Safety, 19 (1978) 205.

[40] Sehmel, G.A., Hodgson, W.H. and Sutter, S.L. "Dry deposition of particles", Pacific Northwest Laboratory Annual Report for 1973 to the USAEC Division of Biomedical and Environmental Research, Part 3, Atmospheric Series, USAEC Report BNWL-1850 (Pt. 3), (1974) p157.

[41] Möller, U. and Shumann, G., J. Geophys. Res., 75 (1970) 3013.

[42] Chamberlain, A.C., Proc. R. Soc. London Ser. A, 290 (1966) 236.

[43] Chamberlain, A.C., Proceed. Royal Soc. London, 296 (1967) 45.

[44] Hinze, J.O., "Turbulence", 2nd Ed., (McGraw-Hill, New York, 1975).

[45] Lin, C.S., Moulton, R.W. and Putnam, G.L., Ind. Engng. Chem., 45 (1953) 636.

[46] Kim, J., Moin, P. and Moser, R., J. Fluid Mech., 177 (1987) 133.

[47] Chapman, D.R. and Kuhn, G.D., J. Fluid Mech., 170 (1986) 265.

[48] Karlsson, R.I. and Johansson, T.G., "LDV Measurements of Higher Order Moments of Velocity Fluctuations in a Turbulent Boundary Layer", in: "Laser Anemometry in Fluid Mechanics", Eds., Adrian R.J. et al., (Ladoan-Instituto Superior Tecnico, Portugal, 1988) p. 273.

[49] Meneveau, C., Lund, T.S. and Cabot, W.H., J. Fluid Mech., 319 (1996) 353.

[50] Gallagher, M.W., Beswick, K.M. and Choularton, T.W., Atmos. Environ., 26A (1992) 2893.

[51] Gaman, A., Rannik, U., Aalto, P., Pohja, T., Siivola, E., Kumala, M. and Vesala, T., J. Atmos. Ocean. Technol., 21 (2004) 933.

[52] Bleyl, M.R., Ph.D. Thesis, Georg-August-Universität, (2001), Göttingen, Germany.

[53] Clough, W.S., Atmos. Environ., 9 (1975) 1113.

[54] Lamaud, E., Brunet, Y., Labatut, A., Lopez, A., Fontan, J. and Druilhet, A., J. Geophys. Res., 99 (1994) 16511.

[55] Lamaud, E., Chapuis, A., Fontan, J. and Serie, E., Atmos. Environ., 28 (1994) 2461.

[56] Chamberlain, A.C. and Chadwick, R.C., Annals App. Bio., 71 (1972) 141.

[57] Nemitz, E., Gallagher, M.W., Duyzer, J.H. and Fowler, D., Quart. J. Royal Meteorol. Soc., 128 (2002) 2281.

[58] Little, P. and Wiffen, R.D., Atmosph. Environ., 11 (1977) 437.

[59] Sutton M.A., Milford C., Nemitz E., Theobald, M.R., Hill, P.W., Fowler, D. et al., Plant Soil, 228 (2001) 131.

[60] Gallagher, W.M., Choularton, T.W., Morse, A.P. and Fowler, D., Quart. J. Royal Meteorol. Soc., 114 (1988) 1291.

[61] Beswick, K.M., Hargreaves, K.L., Gallagher, M.W., Choularton, T.W. and Fowler, D., Quart. J. Royal Meteorol. Soc., 117 (1991) 623.

[62] Pryor, S., Atmos. Environ., 40 (2006) 6192.